Limits on Spin-Independent Couplings of WIMP Dark Matter with a *p*-Type Point-Contact Germanium Detector

H. B. Li,[1] H. Y. Liao,[1] S. T. Lin,[1,2] S. K. Liu,[3] L. Singh,[1,4] M. K. Singh,[1,4] A. K. Soma,[1,4] H. T. Wong,[1,*] Y. C. Wu,[5] W. Zhao,[5] G. Asryan,[1] Y. C. Chuang,[1] M. Deniz,[2] J. M. Fang,[6] C. L. Hsu,[1] T. R. Huang,[1] G. Kiran Kumar,[1] S. C. Lee,[1] J. Li,[5] J. M. Li,[5] Y. J. Li,[5] Y. L. Li,[5] C. W. Lin,[1] F. K. Lin,[1] Y. F. Liu,[1,7] H. Ma,[5] X. C. Ruan,[8] Y. T. Shen,[1] V. Singh,[4] C. J. Tang,[3] C. H. Tseng,[1] Y. Xu,[1,7] S. W. Yang,[1] C. X. Yu,[1,7] Q. Yue,[5] Z. Zeng,[5] M. Zeyrek,[9] and Z. Y. Zhou[8]

(TEXONO Collaboration)

[1]*Institute of Physics, Academia Sinica, Taipei 11529, Taiwan*
[2]*Department of Physics, Dokuz Eylül University, Buca, İzmir 35160, Turkey*
[3]*Department of Physics, Sichuan University, Chengdu 610065, China*
[4]*Department of Physics, Banaras Hindu University, Varanasi 221005, India*
[5]*Department of Engineering Physics, Tsinghua University, Beijing 100084, China*
[6]*Kuo-Sheng Nuclear Power Station, Taiwan Power Company, Kuo-Sheng 207, Taiwan*
[7]*Department of Physics, Nankai University, Tianjin 300071, China*
[8]*Department of Nuclear Physics, Institute of Atomic Energy, Beijing 102413, China*
[9]*Department of Physics, Middle East Technical University, Ankara 06531, Turkey*
(Received 4 March 2013; revised manuscript received 21 May 2013; published 25 June 2013)

We report new limits on a spin-independent weakly interacting massive particle (WIMP)-nucleon interaction cross section using 39.5 kg days of data taken with a *p*-type point-contact germanium detector of 840 g fiducial mass at the Kuo-Sheng Reactor Neutrino Laboratory. Crucial to this study is the understanding of the selection procedures and, in particular, the bulk-surface events differentiation at the sub-keV range. The signal-retaining and background-rejecting efficiencies were measured with calibration gamma sources and a novel *n*-type point-contact germanium detector. Part of the parameter space in the cross section versus WIMP-mass implied by various experiments is probed and excluded.

DOI: 10.1103/PhysRevLett.110.261301 PACS numbers: 95.35.+d, 29.40.Wk, 95.55.Vj

About one-quarter of the energy density of the Universe can be attributed to cold dark matter [1] whose nature and properties are unknown. Weakly interacting massive particles (WIMPs denoted by χ) are its leading candidates. There are intense experimental efforts to study $\chi N \rightarrow \chi N$ elastic scattering via the direct detection of nuclear recoils. Most experimental programs are optimized for mass range at $m_\chi \sim$ 10–100 GeV, motivated by popular supersymmetric models. Germanium detectors sensitive to sub-keV recoil energy were identified and demonstrated as possible means to probe the "low-mass" WIMPs with $m_\chi <$ 10 GeV [2]. This inspired the development of *p*-type point-contact germanium detectors (*p*Ge) with modular mass of kg scale [3].

Our earlier measurements at the Kuo-Sheng Reactor Neutrino Laboratory (KSNL, with a shallow depth of about 30 meter water equivalent) using a four-element array with a total mass of 20 g and analysis threshold of 220 eVee ("ee" denoting electron equivalent energy throughout) have placed constraints on $m_\chi >$ 3 GeV [4]. The CoGeNT experiment reported data with a 440 g detector [5] showing an excess of events at the sub-keV range over the background models. A consistent annual modulation signature was observed. An allowed region in the spin-independent χN couplings ($\sigma^{\rm SI}_{\chi N}$) was derived. Intense interest and theoretical speculations in the low-mass WIMP region were generated [6]. The low energy data of the CDMS and XENON experiments [7] have subsequently excluded the allowed region with different detector techniques, while the original interpretations were defended [8]. It is crucial to have independent experiments which can probe the CoGeNT allowed region and provide further understanding on the detector response and the nature of the sub-keV events in Ge detectors.

We report new results with a *p*Ge of 840 g fiducial mass (actual crystal mass 926 g) at KSNL. The low-background facilities as well as the hardware, trigger, and data acquisition configurations were described in our previous work [4,9]. The detector was enclosed by an NaI(Tl) anti-Compton (AC) detector and copper passive shieldings inside a plastic bag purged by nitrogen gas evaporated from the liquid nitrogen dewar. This setup was further shielded by, from inside out, 5 cm of copper, 25 cm of boron-loaded polyethylene, 5 cm of steel, and 15 cm of lead. This structure was surrounded by cosmic-ray (CR) veto panels made of plastic scintillators read out by photomultipliers. Both AC and CR detectors are crucial, serving both as vetos to reject background and as tags to identify samples for efficiency measurements.

Signals from the point contact are supplied through a reset preamplifier. The output is distributed to a fast-timing amplifier which keeps the rise-time information, and to amplifiers at both 6 and 12 μs shaping time which provide energy information. Signals from the outer surface electrode are processed with a resistive feedback preamplifier and followed by amplifier at 4 μs shaping time. The fast-timing, slow-shaping, and AC-NaI(Tl) output were digitized by flash analog-to-digital converters at 200, 60, and 20 MHz, respectively. The discriminator and timing outputs of the CR panels were also recorded. The physics triggers are provided by the discriminator output of the 6 μs shaping pulses. The trigger efficiency of 100% above 300 eVee was verified by test pulser events. A total of 53.8 days of data were taken, where the data acquisition dead time was 12.6%, measured by random trigger events. Energy calibration was achieved by the internal x-ray peaks and the zero energy was defined with the pedestals provided by the random events. The range in between was cross-checked with pulser events. The electronics noise edge was at 400 eVee.

A cut-based analysis is adopted. There are three categories of selection criteria: (i) the "physics versus noise events" (PN) cuts differentiate physics signals from spurious electronic noise; (ii) the AC and CR cuts identify events with activities only at the pGe target, and (iii) the "bulk versus surface events" (BS) cut selects events at the interior. In addition, the efficiencies and suppression factors (ϵ_X, λ_X) for every selection ($X = $ PN, AC, CR, BS) are measured. They correspond to the probabilities of (signal, background) events being correctly identified. The physics events selected by the PN cuts are categorized by "$\mathrm{AC}^{-(+)} \otimes \mathrm{CR}^{-(+)} \otimes$ B(S)," where $\mathrm{AC}^{-(+)}$ and $\mathrm{CR}^{-(+)}$ represent AC and CR signals in anticoincidence (coincidence), respectively, while B (S) denote the bulk (surface) samples. The χN candidates would therefore manifest as $\mathrm{AC}^{-} \otimes \mathrm{CR}^{-} \otimes$ B events.

Background suppression with the PN, AC, and CR cuts and the evaluations of their respective (ϵ_X, λ_X) follow the well-studied procedures of earlier experiments [4,9,10]. The PN cuts are based on pulse shape characteristics and correlations among the fast and shaping signals. They suppress spurious triggers induced by microphonics effects or the tails of pedestal fluctuations. Background induced by the preamplifier reset is identified by the timing correlations with the reset instant. The *in situ* doubly tagged $\mathrm{AC}^{+} \otimes \mathrm{CR}^{+}$ events serve as the physics reference samples, with which ϵ_{PN} shown in Fig. 2(c) are accurately measured. The majority of the electronics-induced events above the noise edge are identified ($\lambda_{\mathrm{PN}} \sim 1$). The efficiencies for the AC and CR selections are measured by the random events to be, respectively, $\epsilon_{\mathrm{AC}} > 0.99$ and $\epsilon_{\mathrm{CR}} = 0.93$. The suppressions are $\lambda_{\mathrm{AC}} = 1.0$ above the NaI(Tl) threshold of 20 keVee, while $\lambda_{\mathrm{CR}} = 0.92$, measured by reference cosmic samples in which the energy depositions at NaI(Tl) are above 20 MeVee.

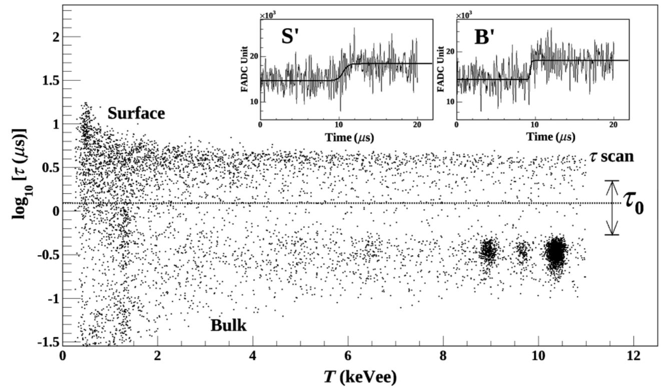

FIG. 1. Scatter plot of the pGe rise time ($\log_{10}[\tau]$) versus energy. The τ_0 line corresponds to the BS cut in this analysis, with τ scan indicating the range of cut-stability test. Typical B′ (S′) pulses at $T \sim 700$ eVee are depicted in the insets.

The BS selection, on the other hand, is a unique feature to pGe. The surface electrode is a lithium-diffused n^+ layer of mm-scale thickness. Partial charge collection in the surface layer gives rise to reduced measurable energy and slower rise time (τ) in its fast-timing output, as compared to those in the bulk region [5,11,12]. The thickness of the S layer was derived to be (1.16 ± 0.09) mm, via the comparison of simulated and observed intensity ratios of γ peaks from a ^{133}Ba source [13]. This gives rise to a fiducial mass of 840 g, or a data size of 39.5 kg days.

The $\log_{10}[\tau]$ versus measured energy (T) scatter plot is displayed in Fig. 1. The boundary between the bulk and surface layers is not well defined, giving rise to events between the two bands. The observed and actual rates are denoted by (B′, S′) and (B, S), respectively. Events with τ less (larger) than τ_0 are categorized as B′ (S′). Typical B′ (S′) events at $T \sim 700$ eVee are shown. At $T > 2.7$ keVee where the τ resolution is better than the separation between the two bands, the assignments B = B′ and S = S′ are justified. At lower energy, (B′, S′) and (B, S) are related by the coupled equations:

$$\mathrm{B}' = \epsilon_{\mathrm{BS}}\mathrm{B} + (1 - \lambda_{\mathrm{BS}})\mathrm{S}, \qquad \mathrm{S}' = (1 - \epsilon_{\mathrm{BS}})\mathrm{B} + \lambda_{\mathrm{BS}}\mathrm{S}, \tag{1}$$

with an additional unitarity constrain B + S = B′ + S′.

The calibration of (ϵ_{BS}, λ_{BS}) involves at least two measurements of (B′, S′) where (B, S) are independently known. The pulser events are inappropriate since their fast-timing output exhibits different pulse shapes from those of physics events. Instead, three complementary data samples, as displayed in Fig. 2(a), were adopted.

(I) Surface-rich events with γ-ray sources. Calibrations with both low and high energy γ sources (^{241}Am at 60 keVee and ^{137}Cs at 662 keVee, respectively) were

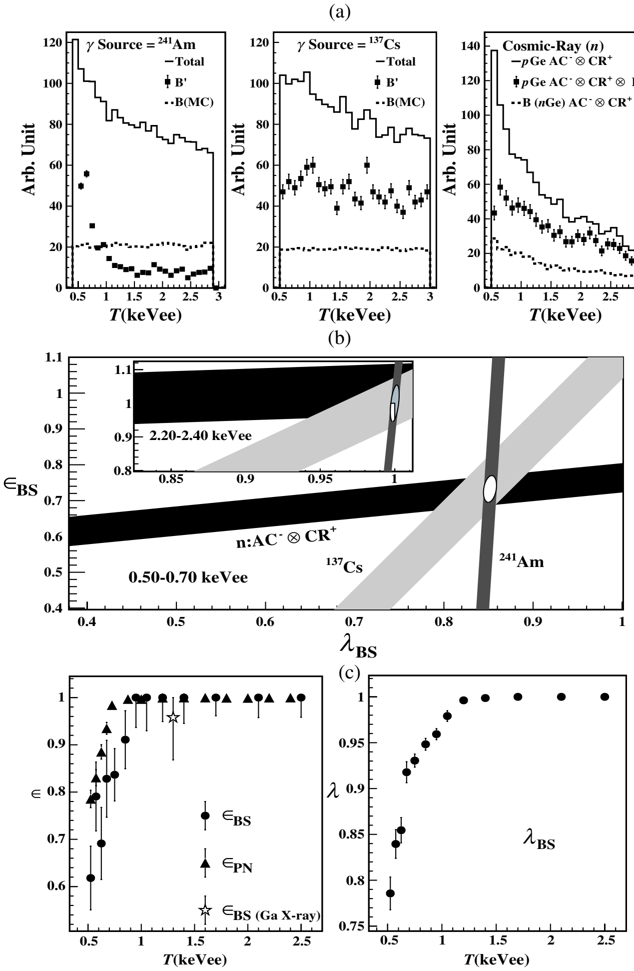

FIG. 2 (color online). The derivation of (ϵ_{BS}, λ_{BS}). (a) The measured total and B′ spectra from pGe with the surface-rich γ-ray (^{241}Am, ^{137}Cs) and bulk-rich cosmic-ray induced neutrons. They are compared to reference B spectra acquired via simulations for γ rays and nGe measurement for cosmic neutrons. (b) Allowed bands at threshold and at a high energy band. (c) The measured (ϵ_{BS}, λ_{BS}) and ϵ_{PN} as functions of energy. Independent measurement on ϵ_{BS} with Ga-L x rays is included.

performed. As displayed in Fig. 2(a), the measured B′ spectra are compared to the reference B derived from full simulation with surface layer thickness of 1.16 mm as input. The simulated B spectra due to external γ sources over a large range of energy are flat for $T < 10$ keVee.

(II) Bulk-rich events with cosmic-ray induced fast neutrons. A 523 g first-of-its-kind n-type point-contact germanium (nGe) detector was constructed. The components and dimensions are identical to those of pGe. The surface of nGe is a p^+ boron implanted electrode of submicron thickness. There are no anomalous surface effects. Data were taken under identical shielding configurations at KSNL. The trigger efficiency was 100% above $T =$ 500 eVee and energy calibration was obtained from the standard internal x-ray lines. The $AC^- \otimes CR^+$ condition selects cosmic-ray induced fast neutron events without associated γ activities, which manifest mostly ($\sim 85\%$) as bulk events. Accordingly, the $AC^- \otimes CR^+$ spectrum in nGe is taken as the B reference and compared with those of $AC^- \otimes CR^+ \otimes B'$ in pGe.

Using calibration data (I) and (II), (ϵ_{BS}, λ_{BS}) are measured by solving the coupled equations in Eq. (1). Standard error propagation formulas are adopted to derive their uncertainties using errors in (B, B′, S′) as input. As examples, the three allowed bands at threshold and at a high energy band are illustrated in Fig. 2(b). The different orientations of the bands are consequences of the different depth distributions of the samples, which give rise to different B:S ratios. The bands have common overlap regions, indicating the results are insensitive to the event locations. The surface-rich γ events and the bulk-rich cosmic-ray induced neutron events play complementary roles in constraining λ_{BS} and ϵ_{BS}, respectively. The results are depicted in Fig. 2(c), with ϵ_{PN} overlaid. By comparing the measured *in situ* Ga-L x-ray peak at 1.3 keVee after BS selection to that predicted by the corresponding K peak at 10.37 keVee, a consistent ϵ_{BS} is independently measured.

The raw spectrum and those of $AC^- \otimes CR^-(\otimes B')$ are depicted in Fig. 3. The peaks correspond to known K-shell x rays from the cosmogenically activated isotopes. The (ϵ_{BS}, λ_{BS})-corrected spectrum of $AC^- \otimes CR^- \otimes B$ is shown in the large inset. Errors above $T \sim 800$ eVee are dominated by statistical uncertainties, while those below have additional contributions from the BS calibration errors of Fig. 2(c), which increase as the efficiencies deviate from unity at low energy. The analysis threshold is placed at 500 eVee, where (ϵ_{BS}, λ_{BS}) ~ 0.5 and the BS selection is no longer valid. The stability of (ϵ_{BS}, λ_{BS}, B′, S′, B) is studied over changes of τ_0 within the τ-scan range

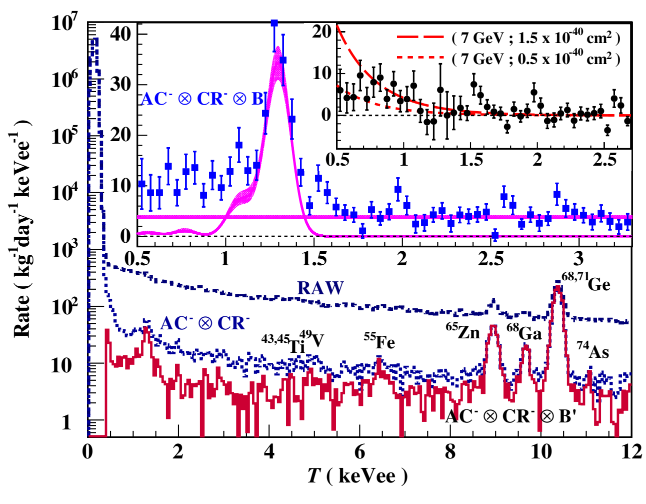

FIG. 3 (color online). Measured energy spectra showing the raw data and those with $AC^- \otimes CR^-(\otimes B')$ selections. The large inset shows the (ϵ_{BS}, λ_{BS})-corrected $AC^- \otimes CR^- \otimes B$ spectrum, with a flat background and L-shell x-ray peaks overlaid. The small inset depicts the residual spectrum superimposed with that due to an allowed (excluded) cross section at $m_\chi = 7$ GeV.

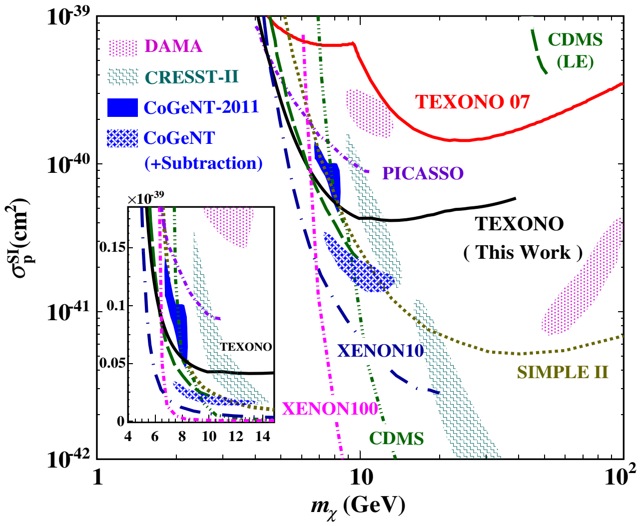

FIG. 4 (color online). Exclusion plot of spin-independent χN coupling at 90% confidence level, superimposed with the results from other benchmark experiments and CoGeNT with and without surface background subtraction.

of Fig. 1. Measurements of B are stable and independent of τ_0, as indicated by the small variations relative to the uncertainties. On the contrary, (ϵ_{BS}, λ_{BS}) exhibit significant shifts in the expected directions. These features indicate that the BS calibration procedures are valid and robust. The systematic errors due to parameter choices are of minor effects to the total uncertainties.

High energy γ rays from ambient radioactivity produce flat electron-recoil background at low energy, as verified by the ^{241}Am and ^{137}Cs spectra of Fig. 2(a), and by the *in situ* $AC^+ \otimes CR^- \otimes B$ spectra. This, together with the L-shell x-ray lines predicted by the higher energy K peaks, are subtracted from $AC^- \otimes CR^- \otimes B$. At a given m_χ, the flat background is measured at an energy range of at least 1.7 keVee and beyond the tail ($< 1\%$) of the χN recoil spectra. The residual spectrum corresponds to χN candidate events and is depicted in the small inset of Fig. 3. Constraints on $\sigma^{SI}_{\chi N}$ are derived via the "binned Poisson" method [14] with conventional astrophysical models [1] (local density of 0.3 GeV/cc and Maxwellian velocity distribution with $v_0 = 220$ km/s and $v_{esc} = 544$ km/s). The event rates of χN spin-independent interaction cannot be larger than the residual spectrum. The quenching function in Ge is derived with the TRIM software which matches well with existing data [10]. As illustration, the χN recoil spectrum due to an allowed (excluded) $\sigma^{SI}_{\chi N}$ at $m_\chi = 7$ GeV is shown in Fig. 3. An exclusion plot of $\sigma^{SI}_{\chi N}$ versus m_χ at 90% confidence level is displayed in Fig. 4. Bounds from other benchmark experiments are superimposed [5,7,15]. The favored region from the CoGeNT data with additional surface background subtraction [6] is included. An order of magnitude improvement over our previous results [4] is achieved. Part of the published DAMA, CRESST II, and CoGeNT allowed regions are probed and excluded. We note that an excess remains in the sub-keV region not yet accounted for in this analysis, the understanding of which is the theme of our ongoing investigations.

Studies continue on pGe and nGe at KSNL. Projects on the improvement of electronics and sub-noise-edge analysis [12] are being pursued. The dedicated dark matter experiment CDEX with sub-keV germanium detectors is taking data at the new China Jinping Underground Laboratory [16]. This facility provides attractive features such as a rock overburden exceeding 2400 m and horizontal drive-in access.

This work is supported by an Academia Sinica Investigator 2011-15 grant, Contract No. 99-2112-M-001-017-MY3 from the National Science Council, Taiwan, and Contract No. 108T502 from TUBİTAK, Turkey.

*Corresponding author.
htwong@phys.sinica.edu.tw

[1] M. Drees and G. Gerbier, Phys. Rev. D **86**, 289 (2012), and references therein.

[2] Q. Yue *et al.*, High Energy Phys. Nucl. Phys. **28**, 877 (2004); H. T. Wong, H. B. Li, J. Li, Q. Yue, and Z. Y. Zhou, J. Phys. Conf. Ser. **39**, 266 (2006).

[3] P. N. Luke, F. S. Goulding, N. W. Madden, and R. H. Pehl, IEEE Trans. Nucl. Sci. **36**, 926 (1989); P. S. Barbeau, J. I. Collar, and O. Tench, J. Cosmol. Astropart. Phys. 09 (2007) 009.

[4] H. T. Wong, Mod. Phys. Lett. A **23**, 1431 (2008); S. T. Lin *et al.*, Phys. Rev. D **79**, 061101(R) (2009).

[5] C. E. Aalseth *et al.*, Phys. Rev. Lett. **101**, 251301 (2008); **106**, 131301 (2011); **107**, 141301 (2011); arXiv:1208.5737.

[6] D. Hooper, Phys. Dark Univ. **1**, 1 (2012); C. Kelso, D. Hooper, and M. R. Buckley, Phys. Rev. D **85**, 043515 (2012), and references therein.

[7] D. S. Akerib *et al.*, Phys. Rev. D **82**, 122004 (2010); Z. Ahmed *et al.*, Phys. Rev. Lett. **106**, 131302 (2011); J. Angle *et al.*, Phys. Rev. Lett. **107**, 051301 (2011); E. Aprile *et al.*, Phys. Rev. Lett. **109**, 181301 (2012); Z. Ahmed *et al.*, arXiv:1203.1309.

[8] J. I. Collar, arXiv:1010.5187; arXiv:1103.3481; arXiv:1106.0653; J. I. Collar and N. E. Fields, arXiv:1204.3559.

[9] H. B. Li *et al.*, Phys. Rev. Lett. **90**, 131802 (2003); H. T. Wong *et al.*, Phys. Rev. D **75**, 012001 (2007); M. Deniz *et al.*, Phys. Rev. D **81**, 072001 (2010).

[10] S. T. Lin *et al.*, arXiv:0712.1645v4.

[11] U. Tamm, W. Michaelis, and P. Coussieu, Nucl. Instrum. Methods **48**, 301 (1967); M. G. Strauss and R. N. Larsen, Nucl. Instrum. Methods **56**, 80 (1967); E. Sakai, IEEE Trans. Nucl. Sci. **18**, 208 (1971).

[12] H. T. Wong, Int. J. Mod. Phys. D **20**, 1463 (2011).

[13] E. Aguayo *et al.*, Nucl. Instrum. Methods Phys. Res., Sect. A **701**, 176 (2013).
[14] C. Savage, G. Gelmini, P. Gondolo, and K. Freese, J. Cosmol. Astropart. Phys. 04 (2009) 010.
[15] R. Bernabei *et al.*, Eur. Phys. J. C **67**, 39 (2010); M. Felizardo *et al.*, Phys. Rev. Lett. **108**, 201302 (2012); G. Angloher *et al.*, Eur. Phys. J. C **72**, 1971 (2012); S. Archambault *et al.*, Phys. Lett. B **711**, 153 (2012).
[16] K. J. Kang, J. P. Cheng, Y. H. Chen, Y. J. Li, M. B. Shen, S. Y. Wu, and Q. Yue, J. Phys. Conf. Ser. **203**, 012028 (2010); Q. Yue and H. T. Wong, J. Phys. Conf. Ser. **375**, 042061 (2012).